Research Article

MONTE CARLO SIMULATION OF NUCLEAR LOGGING DETECTION SYSTEMS

Jadir C. da Silva

Received January 20, 2000 / Accepted June 27, 2001

The utmost challenge in nuclear logs interpretations and spectroscopy comes from the complex and dynamic structure of the radiation detectors response function. To interpret accurately such logs, the energy spectra for several dimensions of nuclear logging detectors must be satisfactorily known. In this work, different incident photon track and energies owing to events occurring into the gamma ray detector are simulated by the Monte Carlo method. The life of a particle within a NaI(Tl) scintillator crystal is computed by simulating the position, direction and energy of electrons and gamma-ray photons interaction by interaction. Four types of photon interactions are computed, namely, photoelectric absorption, pair production, and Rayleigh and Compton scattering. The specific energy loss due to ionization and excitation for electron are also computed. These pulse high spectra are determined by collecting the radiation and transforming it into current pulses. The spectral distribution of these pulses results in a matrix of detector normalized response functions for multiple and complicated source geometry linked with all gamma ray incidence normally required on borehole environment. These data are displayed in such a way that they can be readily carried out into all nuclear log modeling processes with relevant detection effects.

Key words: Monte Carlo Method; Na I (Tl) detector; Nuclear logging.

SIMULAÇÃO MONTE CARLO DOS SISTEMAS DE DETECÇÃO DE PERFILAGEM NUCLEAR - *O grande desafio da interpretação e espectroscopia dos perfis nucleares resulta da estrutura complexa e dinâmica da função resposta dos detectores de radiação. Para interpretar adequadamente tais perfis, os espectros, para várias dimensões de detectores de sistemas de perfilagem nuclear, excitados por fótons de diferentes energias, devem ser conhecidos. Estes espectros são simulados pelo método Monte Carlo, onde a história de uma partícula dentro do cristal cintilador NaI(Tl) é determinada simulando interação por interação, a posição, direção e energia dos elétrons e fótons de raios gama. Quatro tipos de interação dos fótons são simulados: absorção fotoelétrica, produção de pares, e espalhamentos Rayleigh e Compton. As perdas específicas de energia devidas à excitação e ionização de elétrons são também calculadas. Os espectros de altura de pulso são determinados através do recolhimento da radiação e sua transformação em pulsos de corrente. A distribuição espectral destes pulsos resulta em uma matriz de funções respostas normalizadas do detector para múltiplas fontes apresentando geometrias complicadas, relacionadas com todas as formas de incidências de raios gama normalmente requeridas no ambiente de poço. Estes dados são exibidos de tal forma que podem ser facilmente utilizados em todos os processos de modelagem numérica de sistemas de perfilagem nuclear cujos efeitos de detecção sejam relevantes.*

Palavras-chave: *Método de Monte Carlo; Detector Na I (Tl); Perfilagem nuclear.*

Universidade Federal do Rio de Janeiro
Instituto de Geociências – Departamento de Geologia
Prédio do CCMN – Bloco J0
Av. Brigadeiro Trompowski, s/n – Ilha do Fundão
CEP: 21.949 – 900 – Rio de Janeiro – RJ
jadir@geologia.ufrj.br

INTRODUCTION

Nuclear well-logging systems are regarded as a combination of two independent phases, the transport of radiation through the formation and the detection of radiation scattered back into one or more detectors in the probe body. Thus, the following mathematical model can model the nuclear tool performance:

$$\Psi(E) = \int G(E, E')\Phi(E')dE', \qquad (1)$$

where $\psi(E)$ is the detected scattered flux of gamma-ray photons having initially incident energy E' but stretched in a set of energy channels E of the detection system. The kernel $G(E, E')$ on Eq. (1) represents the effects of detection phase taking into account the intrinsic efficiency and energy resolution of the detector. The parameter $\Phi(E')$ is the original incident flux and represents the transport phase.

The NaI (Tl) scintillator crystal coupled to a photomultiplier tube is the most common detector actually used for nuclear logging detection. It shows extremely good light yield, excellent linearity, and a quite good detection efficiency due to the high atomic number of its iodine constituent (Knoll, 1989).

The purpose of this paper to simulate by the Monte Carlo method the history of gamma-ray photons and electrons within the scintillator crystals as those used in the gamma-gamma spectral density and natural gamma-ray spectrometry tool. Much of the focus of this simulation is to get more information about the complex and dynamic structure of the nuclear detector tool response. Each of those particles mentioned can contribute or not to an electric pulse. Although a large number of possible interaction mechanisms are known for gamma-ray photons in matter, only four types play an important role in energy range of nuclear logging services: Rayleigh scattering, photoelectric absorption, Compton scattering and pair production. All these processes lead to the full or partial transfer of energy to electrons in the scintillator crystal, which results in important changes in the gamma-ray history.

All the types of gamma-ray interactions are selected taking into account their relative probabilities of occurrence given by a set of random numbers generated according to the relative cross-sections for each type of interaction (Dickens, 1989). If the selected type of interaction is the Compton scattering, the angles and photon energies after scattering are computed by the Kan (1956) method, which makes the random sampling of the Klein-Nishina distribution (Davisson & Evans, 1952). The azimuthal angle is chosen randomly through the Von Neumann (1951) technique. Having the scattering and azimuthal angles, the direction cosines of the scattered photon can be easily computed.

If the type of interaction selected is the photoelectric absorption, one computes the energy deposited by the photon within the scintillator crystal and the history ends. As a result of the pair production, two annihilation gamma-ray photons appear at the end of the positron track (Knoll, 1989). The history of these photons is simulated in the same way as the primary photons.

Finally, if the choice relies on Rayleigh scattering, one considers a minimum mean energy loss, says 1.0 keV. This scattering is subject to a really small scattering angle, which is repeated until total absorption of photon energy or its reduction to below a certain level. The final response of this phase is the energy loss spectrum of incident photons. The response function of NaI (Tl) detector is finally computed by convoluting the energy loss spectrum with a Gaussian function that simulates the energy resolution effects of both the scintillator crystal and the photomultiplier tube. As result the spectral distribution of these functions will give us a matrix the column of which are the detector normalized response functions.

PROBABILITY FUNCTIONS DESIGN

Radiation transport and interactions are a natural random process suitable for Monte Carlo simulation. This means that the gamma-ray photon and electron directions, energy and position within the NaI (Tl) scintillator crystal are random events, which can be computed by adequate probability distribution functions. As support to the simulations developed in this work I introduce in this section some of these probability distribution functions.

If ρ is a random number in the range [0, 1], one can simulate the mean free path of photons, ℓ, by the

following exponential distribution (Kalos & Whitlock, 1986):

$$\ell = -\frac{1}{\Sigma_T(E)} \ln \rho, \qquad (2)$$

where $S_T(E)$ is the total macroscopic scintillator cross-section for incident gamma-ray photons having energy E.

To simulate equiprobable directions in tridimensional space, Spanier & Gelbard (1969) have introduced the following density function due to Von Neumann (1951):

$$f(\theta,\phi) = \frac{\sin\theta d\theta d\phi}{4\pi}, \qquad (3)$$

where θ and ϕ are polar and azimuthal scattering angles, respectively. This function, Eq. (3), can be represented by the product of two independent distribution functions $f_1(\theta) = \sin\theta d\theta/2$ and $f_2(\phi) = d\phi/2\pi$. This procedure can be simplified by generating a pair of random numbers, ρ_1 and ρ_2, and solving the resulting equations according to the cumulative distribution method (Dickens, 1989):

$$F_1(\theta) = \frac{1}{2}\int_0^\theta \sin t dt = \rho_1, \qquad (4)$$

$$F_2(\phi) = \frac{1}{2\pi}\int_0^\phi dt = \rho_2, \qquad (5)$$

which solution yields $\theta = \arccos(1-2\rho_1)$ and $\phi = 2\pi\rho_2$.

To select the type of gamma-ray interaction, one uses the relative macroscopic cross-section information $\Sigma_k(E)$ for the k-th type of interaction. In Fig. 1 a tagging is shown to choose the type of interaction concerned with each cumulative relative probability of interaction (Dickens, 1989):

$$P_\iota(E) = \frac{1}{\Sigma_T(E)} \sum_{k=0}^{\iota} \Sigma_k(E), \text{ for } \iota = 1, 2, 3 \text{ and } 4, \qquad (6)$$

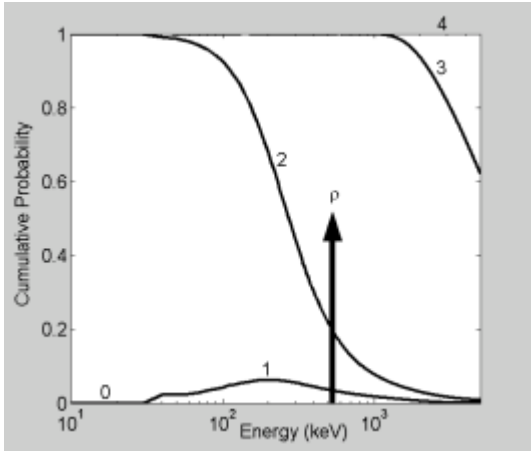

Figure 1 – Tagging to choose the type of photon interaction.

Figura 1 – *Convenção para seleção do tipo de interação dos fótons.*

where $P_0(E) = 0$ and $P_4(E) = 1$. The indexes assumes the forms: i = 1 for Rayleigh scattering, i = 2 for photoelectric absorption, i = 3 for Compton scattering and i = 4 for pair production. The method consists in sampling a random number r in the range [0, 1], represented by the arrow in Fig. 1. Next, this number is compared with the cumulative probabilities of interactions given by Eq. (6). If $P_{i-1}(E) \le \rho \le P_i(E)$, then the selected interaction type is that labeled by index i. Fig. 2 shows, as example, the NaI(Tl) scintillator relative macroscopic cross-sections for all interactions as a function of incident photon energy. It can be seen that for low-energy level, the photoelectric interaction predominates. For medium-energy level, Compton interaction is more important. On the other hand, pair production interactions are only important

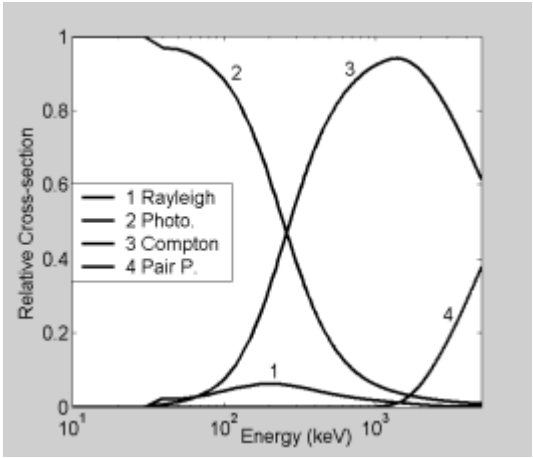

Figure 2 – The NaI(Tl) scintillator relative cross-sections for four main types of photon interactions.

Figura 2 – *Seções de choque relativas do cintilador NaI(Tl) para os quatro tipos principais de interação dos fótons*

for high-energy level and Rayleigh scattering is of little importance.

ENERGY LOSS SPECTRUM

The interaction types of primary concern here take into account the energy range of interest in nuclear logging services. To simulate the transport, scattering, and absorption of individual particles, one must take some representations of the physical principles involved. The probabilities for the types of interactions presented by relative cross-sections have allowed us to compute the scattering angles, photon emission angle, and particle energy distribution. Then the four types of gamma-ray photon interactions are simulated as well as the energy deposition due to secondary particles, which result from the energy loss spectrum of the simulated system.

Compton Scattering

The result of a Compton scattering interaction is the creation of a recoil electron and a scattered gamma-ray photon, the division of energy between the two particles being dependent on the scattering angle (Knoll, 1989). The energy and direction of the scattered photon are computed according to Klein Nishina distributions (Davisson & Evans, 1952). The cosine of polar scattering angle, $\mu = \cos\theta$, and the fraction of incident energy acquired by the secondary photon are computed by Khan's method (1956) which estimates the fraction of energy acquired by the scattered photon per unit of rest electron energy.

The trigonometric functions, $\cos\phi$ and $\sin\phi$, of the azimuthal scattering angle are computed by Von Neumann's technique (1951) according to Eqs. (4) and (5). Having these angles and energy, one computes the direction cosines of the scattered photon. On the other hand, the range $d_{(e^-)}$ of the Compton-scattered electron and its initial energy $E_{(e^-)}$ are computed by Wilson's theory (Spanier & Gelbard, 1969) which establishes that:

$$d_{(e^-)} = \ln 2\left[\frac{E_{(e^-)}}{E_c \ln 2} + 1\right] \qquad (7)$$

where $E_{(e^-)} = E_\gamma - E'_\gamma$ is the electron energy and E_c is a critical electron energy that, in our case, assumes the value:

$$E_c = \frac{1600mc^2}{Z_{ef}},$$

in MeV, where Z_{ef} is the effective atomic number of the scintillator material. So, the following coordinates give the next point of electron interaction:

$$x' = x + d_{(e^-)}\cos\alpha', \qquad (8)$$

$$y' = y + d_{(e^-)}\cos\beta', \qquad (9)$$

$$z' = z + d_{(e^-)}\cos\gamma', \qquad (10)$$

where (x, y, z) is the preceding point and $\cos\alpha'$, $\cos\beta'$ and $\cos\gamma'$ are the direction cosines of the scattered radiation. In order to determine the absorbed energy within the crystal a test is performed to check if the point (x', y', z') lies within the crystal. If the electron path is restricted to the interior of the crystal, the absorbed energy is given by $E_{abs} = E_{(e^-)}$. Otherwise, we have to compute the energy E_1 of the electron when leaving the crystal surface. Let us assume that ℓ' is the projection of the coordinate points x' and y' of Eqs. (8) and (9) on the scintillator crystal radius. Then:

$$\ell' = x'\cos\alpha' + y'\cos\beta'$$

and the radius $r_1 = (x^2 + y^2)^{1/2}$, namely, the projection of the point (x', y', z') of Eqs. (8), (9) and (10) over any plane orthogonal to the crystal axis. The average distance traveled by the electron starting from the face of the crystal to the rest is given by:

$$d_1 = \frac{\ell' - [\ell'^2 + (R_c^2 - r_1^2)(1 - \cos^2\gamma')]^{1/2}}{1 - \cos^2\gamma'}, \qquad (11)$$

where R_c is the crystal radius. If $d_1 < 0$, it is rejected and a new distance follows:

$$d_1 = \begin{cases} z'/\cos\gamma' & \text{if } z' \geq 0 \\ (H_c + z')/\cos\gamma' & \text{otherwise.} \end{cases} \qquad (12)$$

In Eq. (12), H_c is the crystal height. If $d_1 \geq 0$, one computes the difference Δd between the distance effectively traveled by the electron and the distance d_1. Starting from it, one establishes, in agreement with the rejection method, the commitment among the maximum magnitude lost in $d_{(e^-)}$ and the height of the scintillator crystal. This can be summarized of the following way: if $|z + \Delta d\cos\alpha'| \geq H_c$, it is adopted for d_1 the value indicated by Eq. (12). Otherwise, d_1 assumes or the value $d_{(e^-)}$, under assumption that $d_1 > d_{(e^-)}$, or the value given by Eq. (11). Like this, the energy of the electron immediately after leaving the crystal will be given by:

$$E_1 = \exp\left(\frac{d_1}{2.86\ln 2}\right)10.7415. \qquad (13)$$

This analysis allowed us to compute the partial energy loss as being $E_{abs} = E_{(e^-)} - E_1$.

Rayleigh Scattering

In simulating Rayleigh scattering, Khan (1956) supposed that atoms in the scintillator crystal absorb a very small amount of energy (~ 1keV). In this case, the direction of the photon is computed by taking into account the critical angle θ_c defined by:

$$\sin\theta_c = S\frac{mc^2}{E_\gamma}, \qquad (14)$$

where m is the rest mass of electron, c is the light velocity and S is a parameter depending on the scintillator material. Khan (1956) also proposed for Rayleigh scattering the following exponential distribution function:

$$dn \cong \exp(-b\cos\theta_c), \qquad (15)$$

where $b = 1/10$ and critical angle θ_c comes from Eq. (14). In this paper, the cosine of the polar scattering angle, $\mu = \cos\theta$, is simulated as being uniformly distributed in the range [-1, 1], that is:

$$\mu = 2\rho_1 - 1,$$

which is only accepted if $m \geq \cos\theta_c$. Otherwise, we have to repeat this step until this condition is satisfied. Next, $\cos\theta$ is included into the distribution of Eq. (15). Its final acceptance is established by comparing it with a second random number ρ_2, i.e., μ is definitively accepted if $dn \geq \rho_2$, otherwise this step is also repeated until satisfying this condition (Khan, 1956).

Similarly to Compton scattering, the azimuthal angle is computed according to Von Neumann's method (1951), the absorbed energy in the crystal is then 1.0 keV and photon scattering energy is $E'_\gamma = E_\gamma$ - 1.0 keV.

Photoelectric Absorption

Photoelectric absorption is an interaction in which the incident gamma-ray photon disappears. In its place, a photoelectron is produced from the electron shells. Our problem here is to choose the atom in the crystal where the photoelectric effect occurs and outlines the method by which the electron shell is selected. The largest relative probability for the photoelectric effect occurrence relies on the iodine atom due to its relatively high atomic number, compared with that of sodium. Thus, we can consider without appreciable error that the crystal is constituted only of iodine atoms. Knowing that ~80% of the photoelectric absorption occurs in the K-shell, and almost remaining in the L-shell, one can select the reaction shell only by knowing incident photon energy and binding electron energies, E_γ and E_B, respectively. If $E_g \geq 33.16$ keV the reaction occurs in the electron K-shell. If $E_\gamma < 33.16$ keV the reaction occurs in the L-shell. This has allowed us to easily compute the photoelectron energy immediately after its ejection from the selected electron shell, $E_{(e^-)} = E_\gamma - E_B^{(j)}$, where j is the shell label.

The azimuthal and polar electron scattering angles ϕ and θ are uniformly distributed according to Von Neumann's technique (1951) but supporting that polar scattering angle obeys the following distribution:

$$dn = \sin\theta\left[1 + 2\beta\left(1 + \frac{E_B^{(j)}}{E_{(e^-)}}\right)\cos\theta\right]\sin\theta d\theta, \qquad (16)$$

under the assumption that $dn > 0$ for $\beta = \nu_{(e^-)}/c$, where $\nu_{(e^-)}$ is the electron velocity.

Having the azimuthal angle and also polar angles here accepted or rejected according to Eq. (16) concerns, one can compute the direction cosines, $\cos\alpha'$, $\cos\beta'$ and $\cos\gamma'$ and also the next (x', y', z') point of photoelectron interaction. The photoelectron range is computed by the Wilson theory (Spanier & Gelbard, 1969). The analysis of energy deposition within the crystal is made by verifying if the point (x', y', z') lies within the crystal and the same procedure described by the Compton scattering (Eq. 13) is carried out here concerning the Wilson theory (Spanier & Gelbard, 1969).

The vacancy that is created in the electron K-shell is quickly filled by electron rearrangement. The binding energy is liberated in the form of a characteristic X-ray. Considering only the iodine atom, this energy is $E_{R\text{-}X} = E_B^{(K)} - E_B^{(L)} \cong 28.0$ keV and is isotropically distributed. This X-ray is treated similarly to the gamma-ray photon.

Pair Production

This process occurs in the field of the nucleus of the absorbing material. It corresponds to the creation of an electron-positron pair at the point of complete disappearance of the incident gamma-ray photon (Knoll, 1989). For instance, pair production is only energetically feasible when photon energies are greater than $2mc^2$, where the electron and positron energies are given by $E_{(e^-)} = E_{(e^+)} = \frac{1}{2}(E_\gamma - 1.022)$ MeV. The azimuthal angle for electron and positron scattering is uniformly distributed according to Von Neumann 's technique (1951). Polar scattering angle assumes the value $\mu = \cos[mc^2 / E_{(e^-)}]$. An important step of the pair production simulation consists in determining the electron or positron path by the Wilson theory (Spanier & Gelbard, 1969) and also the next interaction point (x', y', z'). Again, one has to check if the end of the particle track lies within the scintillator crystal and all the simulation is repeated like that described for Compton scattering.

As the positron normally deposits all its energy within the crystal two annihilation gamma-ray are emitted in the end of its track. The direction of one of these 0.511 MeV photons is chosen randomly according to the Coveyou (1960) rejection method, which is largely used to select random isotropic direction in tridimensional space. Due to the momentum conservation law, the second annihilation gamma-ray photon is emitted at an angle of 180^0 from the first one.

Main Monte Carlo Simulations Step

The four types of gamma-ray scattering and absorption interactions described above lead to energy deposition in the NaI(Tl) crystal. In order to obtain the energy loss spectra the following steps should be done:

1. Number of history $(N_H) \rightarrow 0$ and Number of interaction $(N_i) \rightarrow 0$;

2. Define all variables linked with incident quantum including energy, initial coordinates (x, y, z) and direction cosines $(\cos\alpha', \cos\beta', \cos\gamma')$ for photon incidence on the lateral surface of the crystal;

3. $N_H \rightarrow N_H + 1$;

4. Compute the mean free path of photons, ℓ, by Eq. (2) and the point (x', y', z') of interaction by a formulae similar to Eqs. (8), (9) and (10) but replacing $d_{(e^-)}$ by ℓ. If point (x', y', z') lies within the crystal goes to step 5; otherwise, return to step 2;

5. Number of interaction $N_i \rightarrow N_i + 1$;

6. If $N_i > 10000$ go to 12;

7. Apply Eq. (6) to select the type of photon interaction;

8. Define the energy imparted among the gamma radiation and/or electron, if it exists;

9. Compute the quantity of electron energy absorbed (E_{abs}) by the scintillator crystal following the formalism given on section "Energy Loss Spectrum" and spans and sums it in its correspondent energy channel;

10. Take all resulting gamma-ray information of step 8, return to step 7 and rebuilt its history until its total disappearance;

11. Return to step 2;

12. Compute the response function of NaI(Tl) detector by convoluting the energy loss spectrum with a Gaussian function that simulates the energy resolution effects;

13. Ends MC simulation.

RESULTS AND DISCUSSIONS

The accuracy of NaI(Tl) scintillator crystal response function is given by two parameters: (1) photofraction and (2) intrinsic efficiency. The photofraction *f* measures the fraction of all photons interacting in the crystal that are totally absorbed, including all the secondary particles. Intrinsic efficiency is the fraction of all photons inciding in the crystal that interacts at least once in it. These parameters can be easily computed when the energy loss spectrum is known. Comparing these parameters with experimental and theoretical data acquired by Franzen and other authors (Kalos & Whitlock, 1986) checks the result of our simulation. As an example of theoretical data, one reports to the program GINASB developed in the *Instituto de Energia Atômica* of São Paulo University. The photofraction and intrinsic efficiency results are shown in Figs. 3(a) and (b) for gamma-ray photon inciding in the frontal face of a 5.08cm x 5.08cm cylindrical scintillator crystal. These results exhibit a quite good agreement with the Monte Carlo results carried out in this paper.

When photofractions results of the MC program are compared, for example, with the *Argone National Laboratory* ANL-6318 experimental data, one finds deviations of 0.44%, 1.82%, 0,57%, 0.36% and 1.25% for incident energies of 0.279 MeV, 0.662 MeV, 1.330 MeV, 2.620 MeV and 4.450 MeV, respectively. The intrinsic efficiency shows deviations of 2.16%, 1,68%, 0.33%, 0.73% and 1.19% at these same energies.

Figs. 4(a), (b) and (c) show the complete structures of energy loss spectra for three monoenergetic gamma-ray sources located 10cm apart from the frontal face of a 5.08cm x 5.08cm cylindrical scintillator. Fig. 4(a) shows the loss spectrum for incident energy of 40 keV, meaning that $E_\gamma << 2mc^2$. This low-energy spectrum shows that the photopeak *A* is accompanied by the iodine characteristic X-ray escape peak B accompanies the photopeak A. This peak lies approximately 28keV below the photopeak. This energy corresponds to the difference between the electrons K- and L-shell binding energies.

In Fig. 4(b) a spectrum is shown for incident energy of 400 keV, which means that $E_\gamma > 2mc^2$. It is

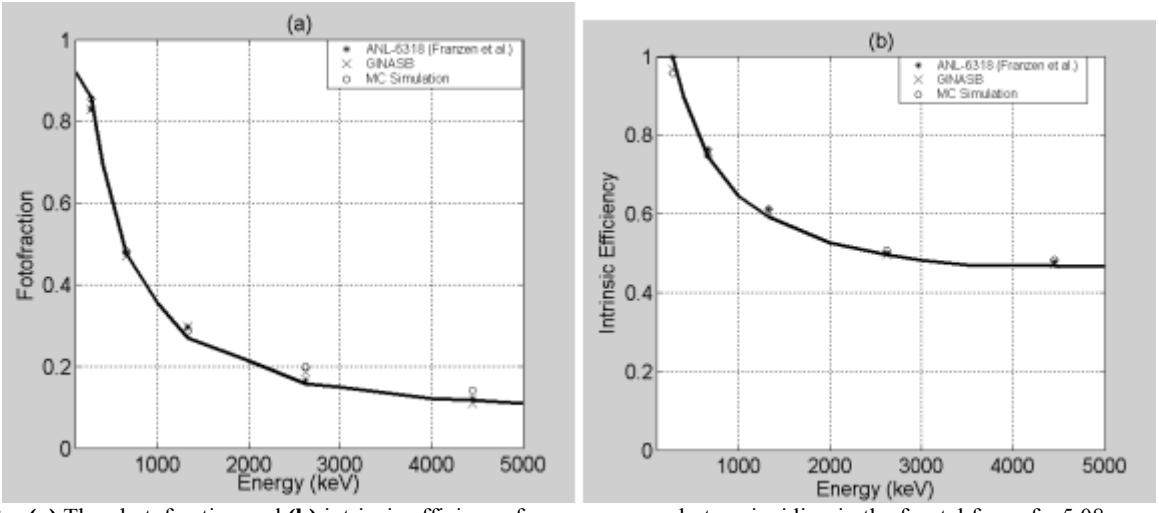

Figure 3 – **(a)** The photofraction and **(b)** intrinsic efficiency for gamma-ray photons inciding in the frontal face of a 5.08 cm x 5.08 cm NaI(Tl) cylindrical crystal.

Figura 3 *– **(a)** Fotofração e **(b)** eficiência intrínseca para fótons de raios gama incidindo na face frontal de um cristal cintilador cilíndrico NaI(Tl) de 5,08 cm x 5,08 cm.*

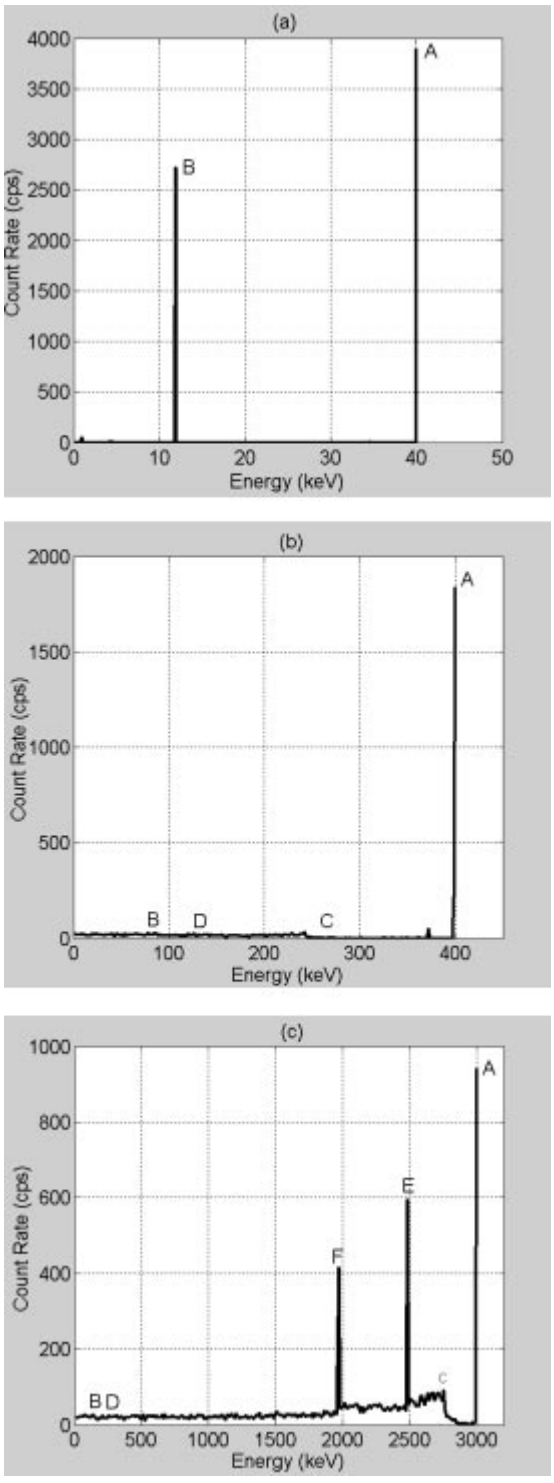

Figure 4 – (a) A low-energy spectrum from a 5.08 cm x 5.08 cm NaI(Tl) scintillator for incident 40 keV gamma-ray photon; **(b)** A medium-energy spectrum from a 5.08 cm x 5.08 cm NaI(Tl) scintillator for incident 662 keV gamma-ray photon; **(c)** A high-energy spectrum from a 5.08 cm x 5.08 cm NaI(Tl) scintillator for incident 3000 keV gamma-ray photon.

Figura 4 – ***(a)*** *Espectro de fótons de raios gama de baixa energia (40 keV) incidindo em um cintilador NaI(Tl) de 5,08 cm x 5,08 cm;* ***(b)*** *Espectro de fótons de raios gama de média energia (662 keV) incidindo em um cintilador NaI(Tl) de 5,08 cm x 5,08 cm;* ***(c)*** *Espectro de fótons de raios gama de alta energia (3000 keV) incidindo em um cintilador NaI(Tl) de 5,08 cm x 5,08 cm.*

seen a full-energy peak *A* due to complete absorption of incident photon energy by photoelectric interaction or multiple Compton scattering followed by photoelectric absorption. The point C is the Compton edge due to photons having a head-on collision. This effect is responsible for the maximum Compton recoil electron energy. Single Compton events followed by Compton escape appear at region B. Region D is due to the continuum single Compton scattering.

Fig. 4(c) shows a spectrum for incident energy of 3000 keV that means that $E_\gamma >> 2mc^2$. The labels E and F in this case identify the new features. Peak E is the single peak escape due to pair production effect in which one annihilation photon leaves the detector without further interaction. This peak appears in the spectrum at energy of 511 keV below the photopeak. Peak F is the double escape peak. It is also due to pair production effect in which both annihilation photons leave the crystal. Therefore it appears at energy of 1002 keV below the photopeak. For the Monte Carlo code regarded here, instead of computing the mean error and the confidence interval for each measurement, one has chosen to establish the number N_i of photon interactions in such form that it results in a mean error less than 1%. If one assumes that the Poisson statistic holds, then this number is obviously $N_i = 10{,}000$ counts. Usually this error is computed by the following expression:

$$e = \sqrt{\frac{f(1-f)}{N_i}}. \qquad (17)$$

Figs. 5(a) and (b) show this error for several energy values inciding into the 5.08cm x 5.08cm and 7.62cm x 7.62cm cylindrical detectors of the gamma-gamma density tool, and into the 5.08cm x 30.0cm cylindrical detector of the natural gamma-ray spectrometry tool. Each of these errors, Eq. (17), is also calculated to test the sensitivity of distinct seeds in generating the series of random events.

These curves show that different seeds do not sensibly alter the results. The reduction of the errors at energies around 250 keV is due to single Compton events followed by Compton escape, which is the predominant effect at this energy. Another important effect in error reduction is the photoelectron escape.

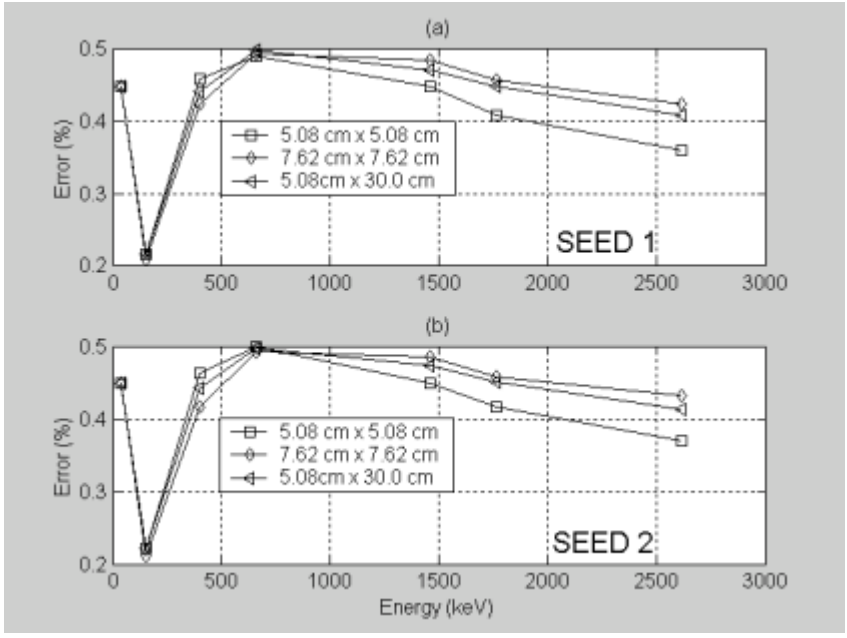

Figure 5 – Error analysis for several energy values inciding into the 5.08 cm x 5.08 cm, 7.72 cm x 7.62 cm and 5.08 cm x 30.0 cm cylindrical detectors also performed to test the sensitivity of distinct seeds ((a) SEED 1 and (b) SEED 2) in generating the series of random events.

Figura 5 *– Análise dos erros para vários valores de energia incidindo em detectores cilíndricos de dimensões 5,08 cm x 5,08 cm, 7,62 cm x 7,62 cm e 5,08 cm x 30,0 cm e teste de sensibilidade à diferentes sementes ((a) SEED 1 e (b) SEED 2) geradoras das séries de eventos aleatórios.*

These and other effects such as scintillator dimension variations can be better observed in Fig. 6 for low-energy levels. It is observed that photofraction decreases near the energy of 250 keV where the Compton scattering predominates over the photoelectric absorption, which has increased the probability of photon escape. Otherwise, at energies below of 120 keV, despite the photoelectric absorption predominance, Compton continuum may effectively disappear and the photofraction increases. Obviously the photofraction value is reduced until energy of 33.16 keV, which corresponds to the absorption edge in which characteristic X-ray is emitted from the electron K-shell of iodine atom and eventually escape from the crystal. Fig. 6 has also shown that photofraction at very low-energy level is almost independent of the crystal dimensions.

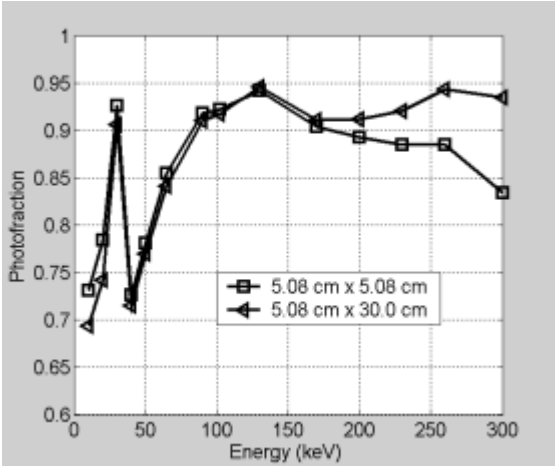

Figure 6 – Effects of scintillator dimension variation in the photofraction for low-energy levels.

Figura 6 *– Efeitos da variação da dimensão do cintilador na fotofração para baixos níveis de energia.*

Energy resolution includes contributions owing to separated effects of charge collection statistic, electronic noise, variations in the detector response over its active volume, and drifts in operating parameter over the course of the measurement. Fluctuations in the photomulplier tube gain from event to event are also included (Knoll, 1989). The energy resolution is defined as:

$$R = \frac{FWHM}{E_0},$$

where *FWHM* is the full width at half maximum of the full-energy peak, and E_0 is the mean pulse height corresponding to the same peak. Figs. 7(a) and (b) show that the resolution effect causes a broadening of

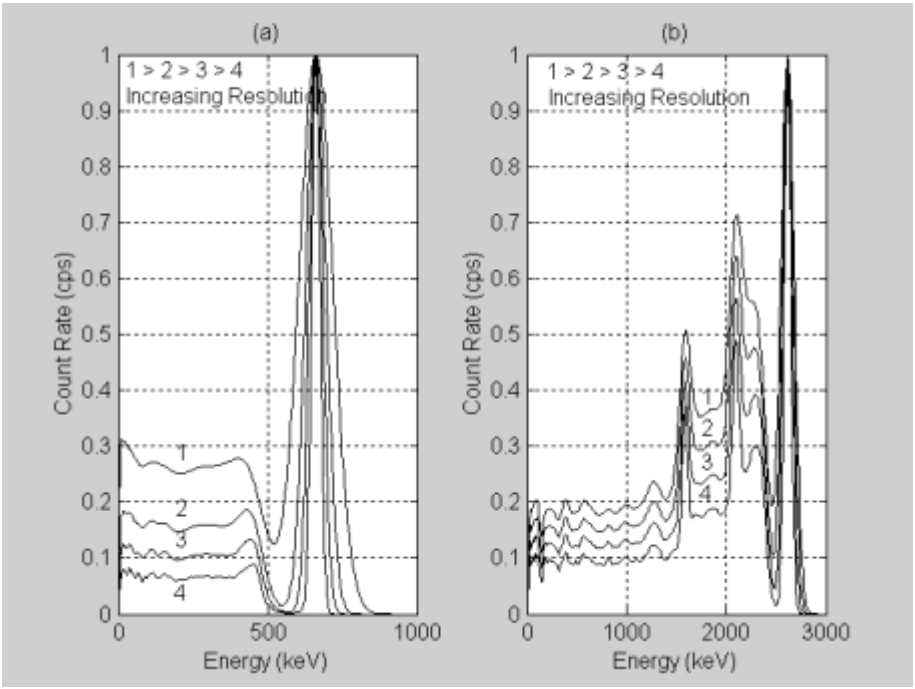

Figure 7 – The broadening of the normalized peaks for (a) medium-energy (662 keV) and (b) high-energy (2615 keV) levels due to resolution effects.

Figura 7 *– Alargamento dos picos normalizados para (a) médio a (b) altos níveis de energia devido aos efeitos de resolução.*

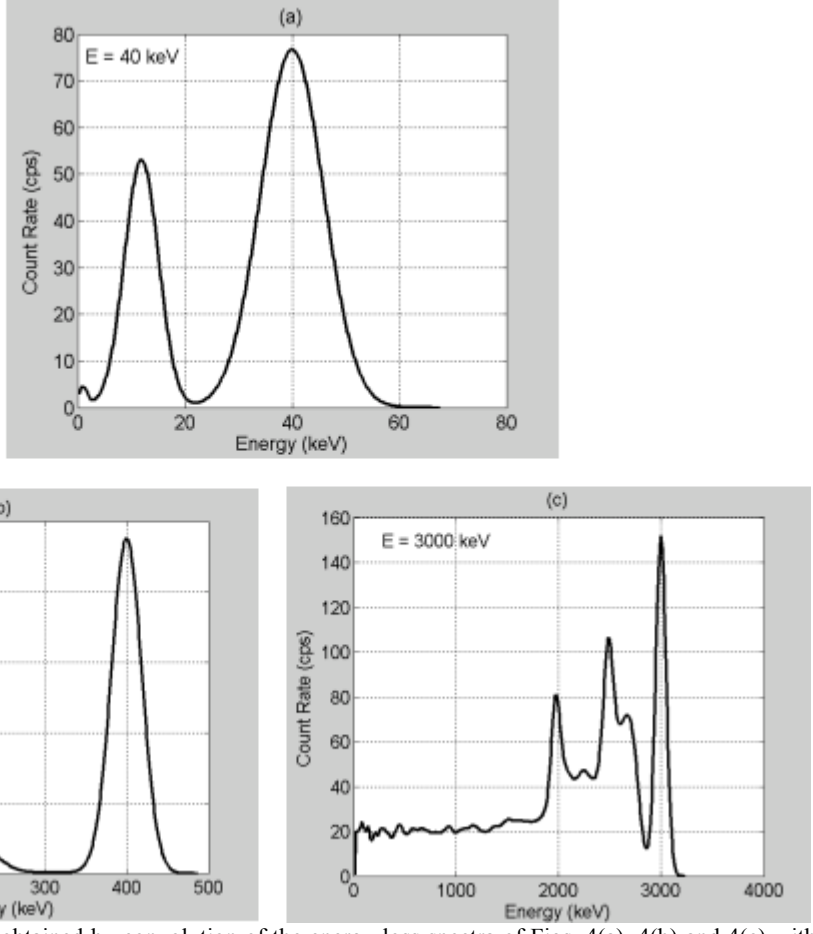

Figure 8 – Detector response functions obtained by convolution of the energy loss spectra of Figs. 4(a), 4(b) and 4(c) with a Gaussian function.

Figura 8 – *Funções respostas do detector obtidas pela convolução dos espectros de perda de energia das Figs. 4(a), 4(b) e 4(c) com uma função Gaussiana.*

normalized peaks. For an assumed Gaussian shape, the *FWHM* is 2.35 times the standard deviation s (Knoll, 1989). The value of σ is dependent on photon incident energy E_γ, being empirically determined by the relationship (Houlung & Kenney, 1991):

$$\sigma(E_\gamma) = A\sqrt{E_\gamma} + B,$$

where *A* and *B* are constants that differ from one detector to another.

Figs. 8(a), (b) and (c) show three detector response functions. All these response functions have been computed by convoluting the energy loss spectra drawn in Figs 4(a), (b) and (c) with a Gaussian function concerning both the crystal and photomultiplier energy resolutions (~8.5% at E_γ = 2615 keV).

In Fig. 9, eight normalized response functions are represented with their locations along the energy channels. Many of the features described in the previous discussion can be observed in these spectra. For instance, all the photons incide in the lateral face of detector. This geometry simulates accurately the wireline nuclear logging. Each of these normalized pulse height spectra represents a column in the energy-concerned matrix of response functions which rows are the scaled energy windows.

CONCLUSIONS

I have shown that the pulse height spectrum of NaI(Tl) detector is the result of multiple and complicated processes for which a new insight may be needed for geophysical applications. Translated into the type of measurement made in well-logging services, almost all difficulties in interpreting these spectra are caused by a profusion of overlapping incidence of photon energies, each of which introducing at the scintillator its own efficiency and resolution effects. Additionally, the pulse high spectrum is subject to other effects associated to the photomultiplier tubes and which was not considered in this work, like degradation by temperature effects and perturbations due to high count rates. There are also non-considered mechanisms by which secondary electrons lose energy by the radiation of bremsstrahlung photons. Apart from these difficulties, the simulation developed in this paper

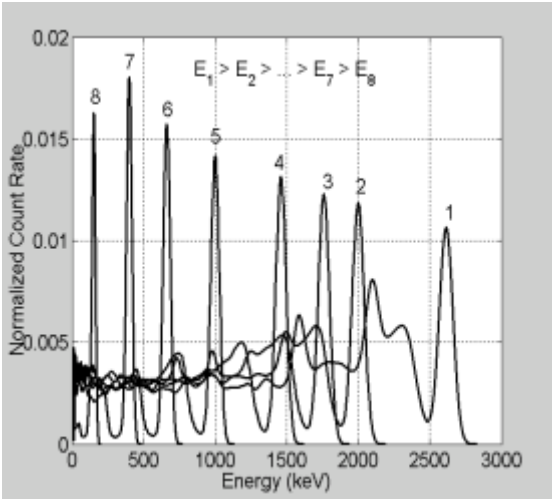

Figure 9 – Examples of normalized response functions for different energies.

***Figura 9** - Exemplo das funções respostas normalizadas para diferentes energies incidentes.*

enables us to satisfactorily construct a matrix the column of which are the NaI(Tl) scintillator normalized response functions concerned with a vast category of gamma-ray sources, their spatial and spectral distributions around the well. If we consider a more detailed analysis of these spectra, it is possible to know more about additional distortions occurring in each pulse height spectrum. This study has recognized the importance in investigating inherent complexity usually found in well-logging detection.

ACKNOWLEDGEMENT

The author thanks the Department of Geology of the Rio de Janeiro Federal University and FAPERJ–Fundação de Amparo à Pesquisa do Estado do Rio de Janeiro through Research Project E-26/171.521/98.

REFERENCES

Coveyou., R. R., 1960. Serial correlation in the generation of pseudo-random numbers. J. Assoc. Comp. Mach, 72(7).

Davisson, C. M. & Evans, R. D., 1952. Gamma-ray absorption coefficients. Review of Modern Physics, **24**(2)**:** 79-107.

Dickens, J. K., 1989. Use of Monte Carlo Techniques to derive yields for $n + C^{12}$ multibody breakup reactions: Programming the computer to simulate collisions by fast neutrons. ORNL, Computer in Physics.

Kalos, M. H. & Whitlock, P. A., 1986. Monte Carlo Methods, Wiley & Sons, New York.

Khan, H., 1960. Applications of Monte Carlo. Rand. Corp. AECU-3259.

Knoll, G. F., 1989. Radiation detection and measurement. John Wiley & Sons, New York, 754pp.

Houlung, L. & Kenney, E. S., 1991. An improvement of Compton scatter imaging with wide aperture detectors – A Monte Carlo study. IEEE Transactions of Nuclear Science, 38(2): 812 – 822.

Spanier, J. & Gelbard, E. M., 1969. Monte Carlo principles and Neutron Transport Problem. Adisson-Wesley, New York.

von Neumann, J., 1951. Various techniques used in connection with random digits. Natl. Bur. Stand, Appl. Math. Series, 36(12).

SIMULAÇÃO MONTE CARLO DOS SISTEMAS DE DETECÇÃO DE PERFILAGEM NUCLEAR

Os sistemas de perfilagem nuclear de poços são considerados como a combinação de duas fases independentes: o transporte da radiação através das formações e a detecção da radiação espalhada que retorna a um ou mais detectores na sonda de perfilagem. Assim, podemos modelar as ferramentas nucleares a partir do modelo matemático a seguir:

$$\Psi(E) = \int G(E, E')\Phi(E')dE',$$

onde $\psi(E)$ é o fluxo detectado de fótons de raios gama apresentando energia inicial E', mas distribuída em uma série de canais de energia E do sistema de detecção. O kernel $G(E, E')$ representa os efeitos da fase de detecção levando-se em conta a eficiência intrínseca e a resolução em energia do detector. O parâmetro $\Phi(E')$ é o fluxo incidente original e representa a fase de transporte. O cristal cintilador NaI(Tl) acoplado a um tubo fotomultiplicador de elétrons é o detector mais comumente usado nas atuais ferramentas de perfilagem nuclear. Ele apresenta uma produção de luz extremamente satisfatória, além de excelentes linearidade e eficiência de detecção devido ao alto número atômico de seu constituinte iôdo (Knoll, 1989). A proposta deste trabalho é simular através do método Monte Carlo a história de fótons de raios gama e elétrons dentro de cristais cintiladores semelhantes àqueles utilizados para aquisições nos perfis de densidade e espectrometria de raios gama naturais. Cada uma destas partículas pode contribuir ou não para um pulso elétrico. Embora exista um grande número de mecanismos possíveis de interação da radiação gama com a matéria, apenas quatro tipos são verdadeiramente importantes no intervalo de energia aplicável aos trabalhos de perfilagem: Espalhamento Rayleigh, efeito fotoelétrico, espalhamento Compton e produção de pares. Todos estes processos levam à transferência total ou parcial de momentum e energia dos fótons para os elétrons no cristal cintilador, o que, obviamente, resulta em importantes mudanças na história dos raios gama. Os tipos de interações descritos acima são selecionados de acordo com a probabilidade relativa de ocorrência de cada um deles. Isto é feito a partir de uma série de números aleatórios gerados em função das seções de choque relativas para cada tipo de interação (Dickens, 1989). Se o tipo de interação selecionado for, por exemplo, o espalhamento Compton, os ângulos e as energias dos fótons após o espalhamento são calculados pelo método de Khan (1956), que faz a amostragem aleatória da distribuição de Klein-Nshina (Davisson & Evans, 1952). O ângulo azimutal é selecionado aleatoriamente através da técnica de Von Neumann (1951). De pose dos ângulos de espalhamento e azimutal, os cossenos diretores dos fótons espalhados podem ser facilmente determinados. Se o tipo de interação selecionado for a absorção fotoelétrica, calcula-se a energia depositada pelo fóton dentro do cristal cintilador e a história termina. Como resultado da produção de pares, dois raios gama de aniquilação aparecem no final do trajeto do pósitron (Knoll, 1989). A história destes fótons é simulada de forma semelhante aos dos fótons primários. Finalmente, se a seleção recair sobre o espalhamento Rayleigh, considera-se uma perda média de energia de 1 keV apenas, visto que este tipo de espalhamento está sujeito a um pequeníssimo ângulo de espalhamento. Neste caso, a história termina ou com a absorção total do fóton, ou a redução de sua energia abaixo de um nível pré-estabelecido, onde não temos mais interesse nele. O resultado final dessa fase é o espectro de perda de energia dos fótons incidentes. A função resposta do detector NaI(Tl) é finalmente calculada convolvendo o espectro de perda de energia com uma função Gaussiana que simula os efeitos de resolução em energia do cristal cintilador e da câmera fotomultiplicadora.

See Note About the Author on page 262.